Transfverter: imbuing transformer-like properties in an interlink converter for robust control of a hybrid ac-dc microgrid

Yunjie Gu, *Member, IEEE*, Yitong Li, *Student Member, IEEE*, Hyeong-Jun Yoo, *Member, IEEE*,
Thai-Thanh Nguyen, *Member, IEEE*, Xin Xiang, *Member, IEEE*, Hak-Man Kim, *Senior Member, IEEE*,
Adria Junyent-Ferre, *Member, IEEE*, Timothy C. Green, *Fellow, IEEE*

Abstract—In a hybrid ac-dc microgrid, stiff voltage sources may appear in either the dc or ac subgrids which gives rise to multiple operation modes as power dispatch changes. This creates a challenge for designing the interlink converter between the ac and dc subgrids since the different modes require different interlink controls. To solve this problem, this paper proposes the concept of a transfverter inspired by how transformers link ac grids. Like a transformer, a transfverter can react to the presence of stiff voltage sources on either the dc or ac side and reflect the "stiffness" and voltage stabilizing capability to the other side. A back-to-back converter with droop control is used as the underlying technology to implement this concept. A novel optimization method called model bank synthesis is proposed to find control parameters for the interlink converter that offer the best controller performance across the different microgrid modes without requiring mode-changing of the controller. The effectiveness of the proposed solution is validated through both simulation and experiments.

Index Terms—Hybrid microgrid, Interlink converter, Transfverter, Model bank synthesis

I. Introduction

Microgrids are evolving from simple dc or ac forms to hybrid ac-dc architectures to account for the diversity of distributed power generation and consumption [1]–[7]. In a hybrid microgrid, an interlink converter links the dc and ac subgrids to share energy and flexibility between them [4], [8]–[12]. The interlink converter is expected to play different roles in various conditions. According to the location of sources, three possible operating modes are apparent for a hybrid microgrid, namely the balanced mode, the dc-dominant mode, and the ac-dominant mode, as illustrated in Fig. 1. In the balanced mode, stiff voltage sources are present in both the dc and ac subgrids, and the interlink converter exchanges

Yunjie Gu, Yitong Li, Xin Xiang, Adria Junyent-Ferre, and Timothy C. Green are with the Department of Electrical and Electronic Engineering, Imperial College London. Hyeong-Jun Yoo, Thai-Thanh Nguyen, and Hak-Man Kim are with Department of Electrical Engineering, Incheon National University. (*Corresponding author: Xin Xiang.*) E-mail: yunjie.gu@imperial.ac.uk; yitong.li15@imperial.ac.uk; hjyoo6580@gmail.com; thanhnteps@gmail.com; x.xiang14@imperial.ac.uk; hmkim@inu.ac.kr; adria.junyent-ferre@imperial.ac.uk; t.green@imperial.ac.uk.

power between the subgrids to balance the overall microgrid. In the dc-dominant mode, however, sources exist in only the dc subgrid, and the interlink converter not only feeds power to the ac grid but also maintains a stiff voltage for the ac subgrid. In such a case, the interlink converter appears as the equivalent of a load on the dc side and a source on the ac side. The ac-dominant mode is just the converse to the dc-dominant mode. A stiff voltage source is defined as the one with a small series impedance (in its Thevenin form) such that the observed voltage changes little with current or power drawn from it. In the case of an ac source, it might also be stiff in terms of frequency such that is frequency changes little with flow of real power.
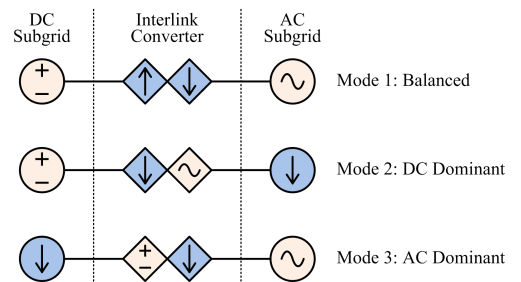

Fig. 1. Operation modes for a hybrid ac-dc microgrid.

The distinction between these three modes is important in the sense that they are related to the control and stability of the interlink converter, since sources and loads have very different dynamic behaviors. Sources usually have a low series impedance to ensure voltage stiffness and stability. Loads, on the other hand, have a high shunt impedance so that their power consumption is not significantly affected by any voltage variation [13], [14]. There should be at least one source in any grid to establish the voltage (and frequency), and the interlink converter must appear as a source to the subgrid with no active sources in itself. Most of the state-of-the-art control schemes for interlink converters are designed for only one of the three modes [8]–[11], that is, appearing as a source only to a particular subgrid and as a load to the other side, which implies risks of instability or inadequate power quality in mode transition. The location of stiff voltage sources could change frequently and suddenly due to the availability of dc generation (such as photovoltaics) and ac generation (such as

combined heat and power plants), outages of the utility grid, or charge/discharge change-over of batteries. It is important that the interlink converter works seamlessly across changing microgrid conditions and especially so during a change of power dispatch or an outage which means that the stiff voltage sources suddenly change from one side to the other and the interlink converter must transfer "stiffness" in the opposite direction. One possible way to do this is to change the control scheme in line with the changing mode, but this needs well-organized coordination throughout the whole microgrid which results in a strong reliance on communication and a low resilience against communication delay, error, or failure [4], [15], [16].

In this paper we propose a robust fixed-structure control scheme for an interlink converter with a single set of control gains which are optimized for well-damped transient responses across all of the three modes of a hybrid microgrid. This is to be achieved without recourse to feedback of remote measurements over communication links. The fixed structure and absence of gain-scheduling means that there is no need to explicitly detect the mode of the microgrid and no need to switch the controller or reset integrators. The proposed solution is inspired by the behavior of a transformer and has therefore been given the portmanteau name "transfverter" through combining "transformer" and "converter". Like a transformer, a transfverter can react to the presence of a voltage source on either side and transfer the stiffness (low output impedance and high inertia) of that source to the other side regardless of where the source is located. A back-to-back converter with droop control on both the dc and ac sides is used as the underlying technology to implement this concept. The set-points of the droop control are regulated by an upper controller to correct the droop control error and maintain the balance of the hybrid microgrid overall. This upper controller needs a choice of control structure and parameters that are robust to mode changes, which gives rise to a robust control problem for structural uncertainty. To solve this problem, a novel optimization algorithm called *model bank synthesis* will be introduced, which can search for a control gain matrix to optimize the worst-case scenarios across multiple modes.

The paper is organized as follows. The concept of transfverter and its general implementation is explained in Section II. The principle of model bank synthesis and its application in optimizing transfverters is described in Section III. Section IV provides the simulation and experiment verifications. The last section concludes this paper.

II. TRANSFVERTER

The key function of a transfverter is the autonomous transfer of stiffness across an ac-dc microgrid. As illustrated in Fig. 2, it can react to the presence of voltage sources on either side and transfer the grid supporting effect to the other subgrid of the hybrid microgrid to ensure stable operation wherever the sources are located.

The converter topology and control structure to implement the transfverter concept is shown in Fig. 3. A pair of converters, one dc-dc and one dc-ac, are connected back-to-back

and buffered by an interlink capacitor. Both converters have independent fast inner-loop voltage control so that they each may appear as a stiff voltage source and support voltage stability. The voltage control scheme in [17], [18] is used but not described in detail here since it is not the focus of this paper. It suffices to point out that the voltage control makes the converters act as voltage sources with predefined series impedance [19], [20]. The set-point of the voltage sources are governed by droop control so that the transfverter may share power with other sources in each subgrid. Power-voltage (P-V) and power-frequency (P-F) droop control are used for the dc-dc and dc-ac converters respectively to govern the dc voltage and ac frequency set-points (v_{dc}^* and f_{ac}^*), as shown in Fig. 4. D_{dc} and D_{ac} are P-V and P-F droop coefficients, and low pass filters (LPFs) are used to attenuate noise and provide virtual inertia [21], [22]. Inductive virtual impedance is embedded in the ac-side inner-loop voltage control to reduce P-V coupling and enhance P-F droop controllability [23], [24]. The virtual impedance itself enables reactive power sharing so Q-V droop control is not necessary and the ac-side voltage reference v_{ac}^* is determined by frequency f_{ac}^* alone [20]. On top of the droop control, an overarching interlink controller regulates the droop power set-points P_{dc}^* and P_{ac}^* to stabilize the interlink capacitor voltage and balance the power flow between the dc and ac subgrids.
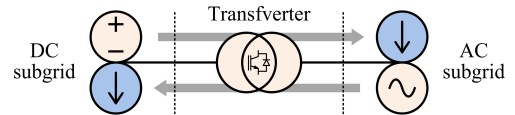

Fig. 2. The concept of a transfverter: transferring stiffness autonomously in an ac-dc microgrid.
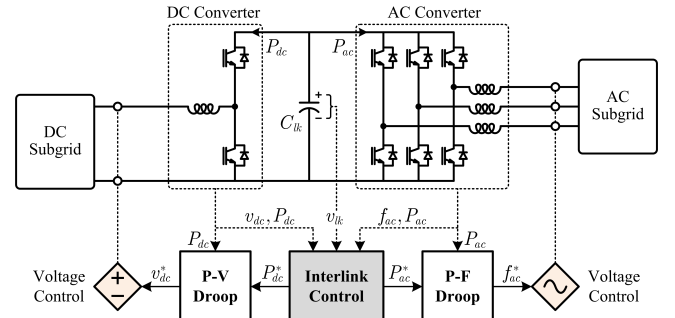

Fig. 3. Overall control architecture to implement the transfverter concept on a pair of back-to-back dc-dc and dc-ac converters.
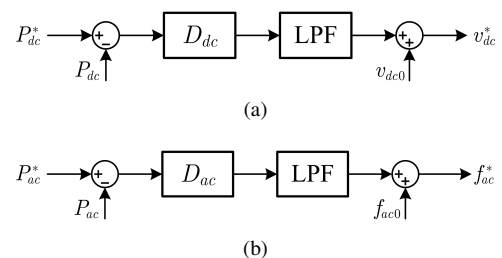

Fig. 4. Droop control schemes in Fig. 3. (a) P-V droop on the dc side. (b) P-F droop on the ac side.

The physical resemblance between a transfverter and a transformer is illustrated in Fig. 5. The behavior of a transformer is governed by the flux linked to the mutual inductance X_m which creates electromotive forces (EMFs) E_1 and E_2 in each winding in proportion to each other. The flux is in turn influenced by the voltage at each of the winding terminals. If a stiff voltage source (i.e., a voltage source with a small series impedance) is connected to one winding, then the EMF in that winding is forced to follow that applied voltage and the EMF in the other winding therefore becomes stiff. This happens in a symmetrical fashion, that is, a stiff source on either side creates stiffness on the other side. The transfverter replicates this behavior and transfers stiffness from ac side to dc side or vice versa without having to be programmed to assume one side is stiff or detect stiffness and change modes. This is achieved by a symmetrical voltage control architecture with two controlled voltage sources v_{dc}^* and v_{ac}^* on both the dc and ac sides. The voltages are created by the switching of the voltage on the interlink capacitor C_{lk}, which in turn is charged by the voltage applied on either the dc or ac terminal. If a stiff voltage source is connected to one side, then this side dominates the interlink voltage regulation, and the other side takes the regulated interlink voltage to form a stiff source on its own side. As a result, a transfverter enables bidirectional and seamless transfer of voltage stiffness just like a transformer, as highlighted by the blue arrows in Fig. 5 (the direction of the arrows denotes the transfer of voltage stiffness, rather than physical power flow). In comparison, prior-art control for the interlink converter only supports uni-directional stiffness transfer. In the example in Fig. 5(c), the dc side is voltage-controlled (low impedance), but the ac side is current-controlled (low admittance), and the interlink capacitor voltage is solely regulated from the ac side. As a result, the voltage stiffness can only be transferred from the ac to the dc side, as marked by the orange arrows. This implies that the microgrid would be vulnerable to ac voltage collapse in Mode2 (dc dominant) with no stiff voltage sources in the ac subgrid. It is worth noting that the stiffness of the ac voltage is in the sense of both magnitude and frequency, which can be jointly reflected by a generalized impedance [25] to match the symmetrical illustration in Fig. 5.

Like transformers, multiple transfverters can be connected in parallel without communication, since the droop control with virtual series impedances on both sides naturally mitigates circulating currents and enables power sharing. This property facilitates modular and scalable design which provides extra flexibilities in manufacturing, maintenance and upgrading.

Now we discuss the detailed control scheme and parameters for the transfverter. The inner-loop and droop control have been well-understood and have standard design procedures [26]. The overarching interlink control, on the other hand, is a new problem arising from the transfverter concept. The interlink controller has multiple tasks: (i) balancing the interlink capacitor voltage (v_{lk}); (ii) matching the dc voltage and ac frequency of the hybrid microgrid; (iii) mitigating the transient deviation of dc and ac voltage/frequency (v_{dc} and f_{ac}) in load disturbances. These tasks may be in conflict with
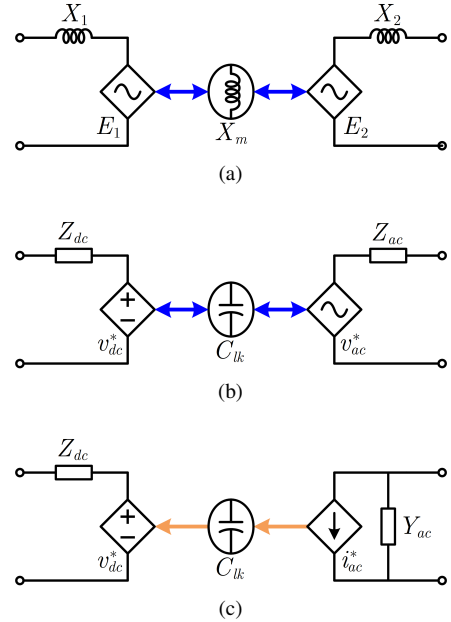

Fig. 5. Illustration of the resemblance between a transformer and a transfverter, and their differences to prior-art solutions: a transformer and a transfverter enable bidirectional transfer of voltage stiffness; but prior-art solutions only support uni-directional transfer. Note the arrows in this figure indicate the direction of "stiffness transfer", not the direction of physical power flow. (a) Transformer. (b) Transfverter. (c) Prior-art interlink control.

each other. For example, tight control over v_{dc} may sacrifice the performance of f_{ac}, and tight control over v_{dc} and f_{ac} may induce higher variation of v_{lk}. This causes a difficulty for designing the interlink control scheme.

What adds to the difficulty is that the dynamic properties of a hybrid microgrid may vary suddenly and drastically in mode transition, potentially making an interlink controller fine-tuned for one mode unstable or poorly damped for another. To illustrate this, the frequency responses of a typical ac-dc microgrid (configuration given in Section IV) from P_{dc}^* to P_{dc} and v_{dc} in the dc- and ac-dominant modes are drawn in Fig. 6(a). It is clear that in the dc-dominant mode, there is a high gain from P_{dc}^* to P_{dc} and a low gain from P_{dc}^* to v_{dc}, and the ac dominant mode has just the opposite response. This is because v_{dc} is clamped by the dc subgrid in the dc dominant mode, and P_{dc} is clamped by the dc loads in the ac-dominant mode. Similar phenomena are observed for the frequency response from P_{ac}^* to P_{ac} and f_{ac} as well, as shown in Fig. 6(b). As a result of these changes in the physical plant, the interlink controller faces significant uncertainty which calls for a robust control scheme. H_∞ control is a well-known solution for robust control but is infeasible for our problem, since our difficulty arise from structural uncertainty (different modes for the hybrid microgrid), rather than parameter uncertainty (the perturbation of parameters in a single mode) [27]. There is not an effective way to represent model variation caused by structure uncertainty in terms of H_∞ norm which is the starting point of H_∞ control. To tackle this challenge, we propose a novel robust controller optimization algorithm called model bank synthesis.

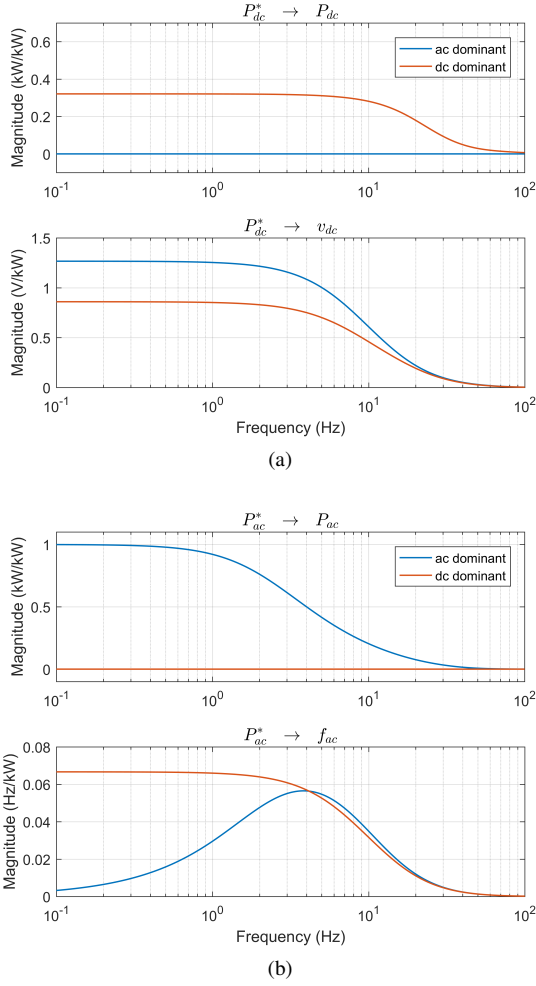Before giving the mathematical development, it may help

Fig. 6. Control gain from power reference to power in dc-dominant and ac-dominant modes. (a) P_{dc}^* to P_{dc} and v_{dc}. (a) P_{ac}^* to P_{ac} and f_{ac}.

the readers to offer an intuitive interpretation of how the interlink controller works. To serve this purpose, we first present a simple proportional-integral (PI) control scheme for interlink control, which will then be generalized and placed in a framework for optimizing the robustness to structural uncertainty in the next section.
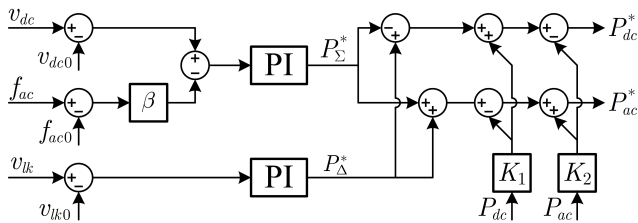

Fig. 7. PI control scheme for interlink control in Fig. 3.

In this PI control scheme, shown in Fig. 7, the interlink controller is divided into two control loops (see Fig. 3 for the reference power direction). The first loop sets the net power flow P_Σ^* from dc to ac subgrid to balance the hybrid microgrid as a whole. This loop is designed to match the voltage error on the dc side ($v_{dc} - v_{dc0}$) to the frequency error on the ac

side ($f_{ac} - f_{ac0}$). As v_{dc} and f_{ac} reflect the power balances in the dc and ac subgrids respectively according to the P-V and P-F droop control, such a matching serves as a linkage for the power balance in the entire hybrid microgrid and is called hybrid droop control [8]. The matching coefficient $\beta = D_{dc}/D_{ac}$ is set to compensate for the difference in the droop coefficients D_{dc} and D_{ac}. The PI controller acts on ($v_{dc} - v_{dc0}) - \beta \cdot (f_{ac} - f_{ac0}$) and settles to the following equilibrium:

$$v_{dc} - v_{dc0} = \beta \cdot (f_{ac} - f_{ac0}) \qquad (1)$$

where the variables denoted by the subscript "$_0$" represent the corresponding nominal values. As a result, the first control loop serves as an arbitrator to equalize the voltage deviation and frequency deviation on the dc and ac sides, on top of which secondary control can be deployed to further mitigate the deviations [1]. The second control loop adds a power offset P_Δ^* to regulate the voltage of the interlink capacitor which may otherwise deviate due to mismatch between P_{ac} and P_{dc} caused by regulation errors and power losses. This loop uses another PI controller to act on the interlink voltage error $v_{lk} - v_{lk0}$, so that the equilibrium satisfies:
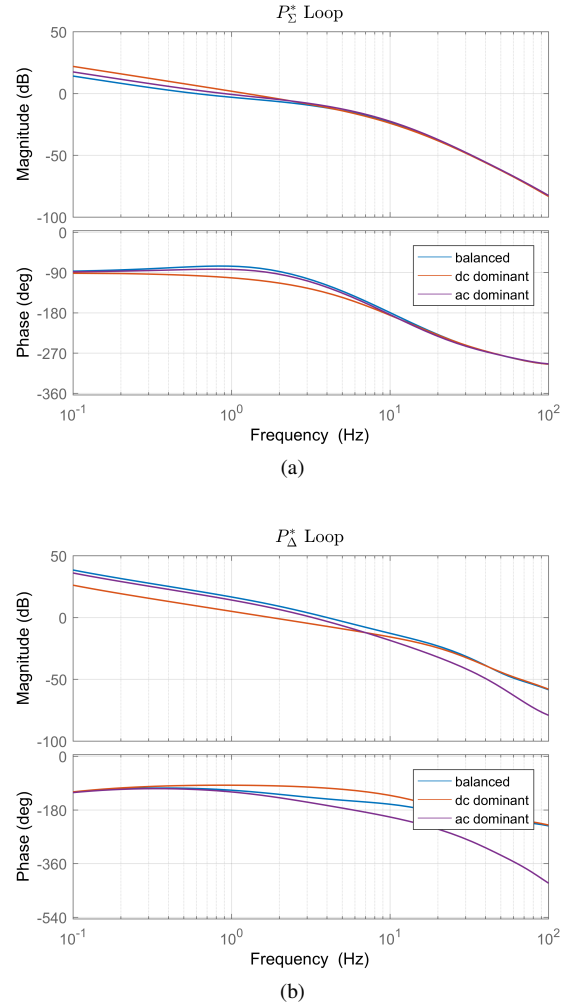
$$v_{lk} = v_{lk0}. \qquad (2)$$

(a)

(b)

Fig. 8. Open-loop frequency response for two PI loops in three modes. (a) P_Σ^* loop. (b) P_Δ^* loop.

Since the function of these two PI loops are nearly decoupled, they could be configured independently as two single-input-single-output (SISO) systems. To ensure the controller works well for all microgrid modes (balanced, dc-dominant and ac-dominant), the open-loop frequency response for each loop in each mode is drawn in Fig. 8 and the PI parameters are designed to ensure adequate closed-loop phase margin for all modes. The feed-forward paths from P_{dc} and P_{ac} help to speed-up dynamic response and the feed-forward gain is set to $K_1 = K_2 = 1/2$. This control scheme provides a simple solution covering the basic functions of the transfverter, and can be used as the initial point for the model bank synthesis to be discussed in the following.

III. MODEL BANK SYNTHESIS

The preceding section presents a heuristic PI-based interlink controller, which is intuitive but inaccurate and suboptimal. This section introduces an algorithm called model bank synthesis to optimize the controller for the best trade-off between multiple operation modes. This algorithm also provides a general robust control solution for systems with multi-model structural uncertainty and can be readily migrated to other applications beyond microgrids.

The essential idea for model bank synthesis is to collect the models for different modes into an extended model, the model bank, and optimize them all together. As shown in Fig. 9, the problem is formulated as a set of models G_m with a series of external disturbances w_n, performance evaluators z_l, controlled input u, and measured output y, and the cost function f to be minimized is defined as

$$f(l, m, n, K) = \|z_l(G_m, w_n, K)\| \quad (3)$$

in which $z_l(G_m, w_n, K)$ is the response of the lth performance evaluator z_l for the mth model G_m under the nth disturbance w_n and the feedback control gain K. The norm operator $\|\cdot\|$ can be set by the designer and we use the most commonly used L_2 norm in this paper. For an unstable system, the norm is set to infinity which ensures the stability of the system throughout the optimizing process. The optimization target is to find K to minimize $f(l, m, n, K)$ in the worst combination of (l, m, n).

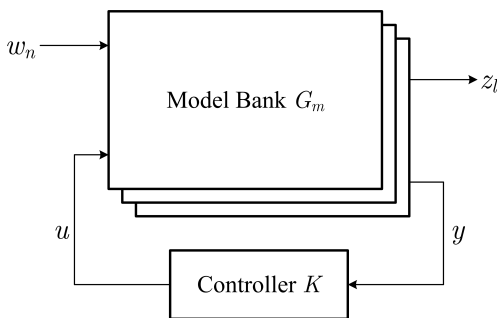$$K_\star = \arg\min_{K} \max_{l,m,n} f(l, m, n, K). \quad (4)$$

Fig. 9. Problem formulation of model bank synthesis.

Equation (4) defines a MinMax optimization problem, that is, minimizing the maximum possible cost [28]. If $f(l, m, n, K)$ is convex, a global optimal solution can be found with sub-gradient descent method [29]. As illustrated in Fig. 10, the optimal point lies on the intersection of multiple cost functions, and the solver switches among these functions to approach the optimal point along the gradient direction. The detailed procedure is described in Algorithm 1. At each step t, the solver first traverses through all feasible (l, m, n) to identify the maximum of $f(l, m, n, K_t)$ for the current solution K_t, and denotes this maximum as (l_t, m_t, n_t). The gradient $g_t = \partial f / \partial K$ is then calculated at (l_t, m_t, n_t, K_t), and K is updated according to $K_{t+1} = K_t + \gamma_t \cdot g_t$. The step size γ_t is dynamically reselected to ensure that $|f_{t+1} - f_t| < \eta|f_t|$ so that f_t does not jump too far in each step, in which η is a small positive coefficient, and $f_t = f(l_t, m_t, n_t, K_t)$. The iteration stops when $|f_{t+1} - \min_t(f_t)| < \epsilon$ (ϵ is a small positive threshold) for several consecutive steps, meaning that the descent of f_t has ceased.

Algorithm 1 Sub-gradient descent for MinMax optimization

1: $t \leftarrow 0$, initialize K_0, γ_0
2: **repeat**
3:    $(l_t, m_t, n_t) \leftarrow \arg\max\limits_{l,m,n} f(l, m, n, K_t)$
4:    $f_t \leftarrow f(l_t, m_t, n_t, K_t)$
5:    $g_t \leftarrow \frac{\partial f}{\partial K}\Big|_{l_t, m_t, n_t, K_t}$
6:    $\gamma_t \leftarrow \min(\gamma_0, f_t/\|g_t\|)$
7:    $K_{t+1} = K_t + \gamma_t \cdot g_t$
8:    $t \leftarrow t + 1$
9: **until** $|f_{t+1} - \min\limits_t(f_t)| < \epsilon$ for consecutive T steps
10: **return** K_t for minimum f_t

In order to apply the model bank synthesis to the interlink control of the transfverter, we rearrange the PI controller in Fig. 7 to match the formulation in Fig. 9, as shown in Fig. 11. The model for the hybrid microgrid is linearized around the equilibrium point. The two integrators (ξ_{hb} and ξ_{lk}) are carried over from the two PI control loops in Fig. 7 to eliminate steady-state error. All seven measurable variables (e_{dc}, e_{ac}, e_{lk}, ξ_{hb}, ξ_{lk}, P_{dc}, and P_{ac}) are fed to the interlink controller to provide as complete as possible feedbacks that is useful for generating the optimal control actions on P_{dc}^* and P_{ac}^*, which results in a 2×7 gain matrix K. The external disturbance w is modeled as load perturbation on dc and ac sides (P_{ldc} and P_{lac}), and three performance evaluators are used that represent the deviation of dc voltage (e_{dc}), ac frequency (e_{ac}), and interlink capacitor voltage (e_{lk}). The deviations are normalized
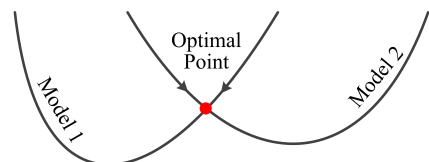

Fig. 10. Sliding on multiple cost curves along the gradient direction to search for the overall optimal point.

by the weights below:

$$W_{dc} = (P_0 \cdot D_{dc})^{-1}, \ W_{ac} = (P_0 \cdot D_{ac})^{-1}, \ W_{lk} = (\rho \cdot v_{lk0})^{-1}. \tag{5}$$

in which P_0 is nominal power of the interlink converter and ρ is the maximum allowed percentage of interlink capacitor voltage variation. These weights are set as the reciprocals of the corresponding maximum variation range to place equal importance on e_{dc}, e_{ac}, and e_{lk}. W_{dc} and W_{dc} are consistent with the matching coefficient β in Fig. 7 and (1), that is, $\beta = D_{dc}/D_{ac} = W_{dc}/W_{ac}$.
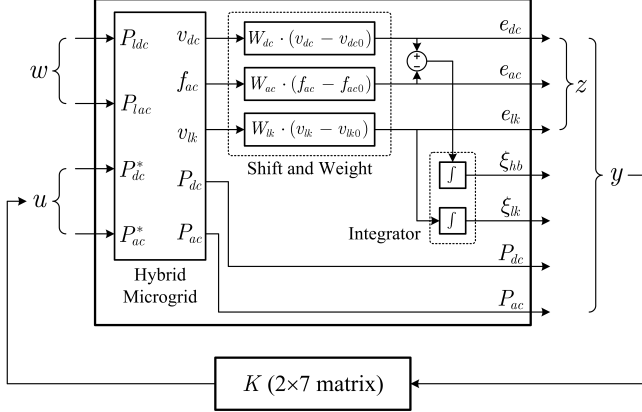

Fig. 11. Rearranging the PI control in Fig. 7 to fit the general form in Fig. 9. The "Shift and Weight" blocks correspond to the error comparisons in Fig. 7, the "Integrator" blocks correspond to the integral parts of the PI controllers in Fig. 7, and the gain matrix K is a generalization of the PI gains and feed-forward gains in Fig. 7. These three blocks compose the overarching "Interlink Control" in Fig. 3, and the "Hybrid Microgrid" block represents the physical model of the hybrid ac-dc microgrid and the interlink converter with inner-loop and droop control. The three modes of the hybrid microgrid give rise to three models to be put in the model bank (Fig. 12), and K is optimized for the overall performances across all three modes via model bank synthesis.
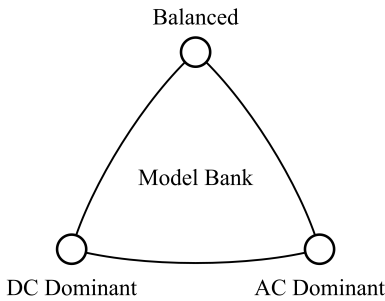

Fig. 12. The three operation modes for the hybrid ac-dc microgrid give rise to three models in the model bank.

For each of the three modes for the hybrid microgrid (balanced, dc-dominant and ac-dominant, shown in Fig. 12), we formulate a model as in Fig. 11, and put all three models into the model bank. Using the model bank synthesis, K is optimized to minimize e_{dc}, e_{dc}, and e_{dc} under load disturbances P_{ldc} and P_{lac} in the worst case. Impulse responses are used to represent disturbance responses since they contains rich transients in all frequencies. The problem may not be convex so global optimization is not guaranteed with sub-gradient

descent, but the risk could be mitigated by carefully choosing the initial parameter K_0. We set K_0 in consistent with the PI gains and feed-forward gains in Fig. 7 so that optimization can be conducted on top of the conventional frequency-domain control design methodology (Fig. 8).
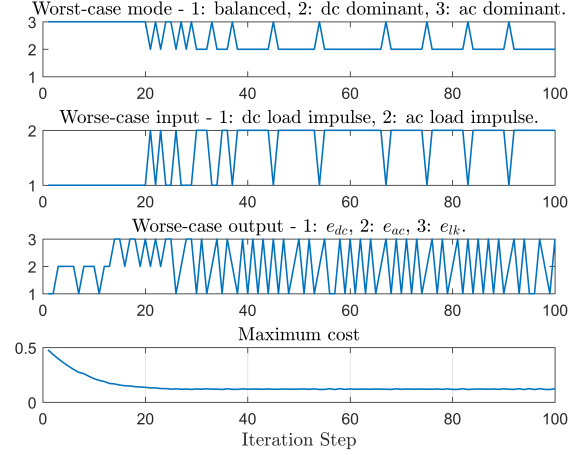

Fig. 13. Cost reduction and worst-case switching in iteration process. The meaning of the vertical axes are explained above each sub-figure. For example, for the top sub-figure, the vertical axis stands for three microgrid modes (1: balanced, 2:dc dominant, 3:ac dominant) associated to the worst case during iteration.

The iteration process can reveal much interesting information. We use the hybrid microgrid configuration in Section IV to run a case study and show the results that follow. In Fig. 13, it is clear to see that the worst-case mode switches between Mode2 (dc dominant) and Mode3 (ac dominant) during the iteration. This can be understood from the fact that the microgrid in Mode1 (balanced) is powered by stiff sources on both dc and ac sides which can self-sustain even without the interlink converter, but Mode2 and Mode3 rely solely on the interlink converter to stabilize the subgrid with no stiff sources. The interlink control actions to stabilize the two modes are different (and even opposite), so the optimization algorithm switches in between to find the best overall controller. For each of the worst-case modes, the worst output (e_{dc}, e_{ac}, e_{lk}) also switches, indicating the need for a trade-off between different control targets: stabilizing dc voltage, ac frequency, and interlink capacitor voltage, which matches the discussion in Section II. The maximum cost generally reduces due to the effect of gradient descent, but there is also a small ripple observable in the cost which is caused by the overshoot in worst-case switching. The cost finally converges to around 0.1 at the end of the iteration process, indicating that an equilibrium of the control performance for all modes has been achieved. Compared to the initial cost 0.5, the final cost 0.1 indicates that the optimized controller improves the disturbance response five times under the worst-case scenarios.

Fig. 14 shows the performances when different model banks are used for the optimization. If the model bank only contains Mode2 (denoted as Model(2) in the figure), the performance for this particular mode is improved, but Mode3 oscillates more than the model bank synthesis. In comparison, the model bank containing all the modes (denoted by Model(1,2,3))

provides the best overall performance. These results show that the model bank synthesis offers the best trade-off between different modes. Similar results can be found if the model bank only contains Mode3, but are not displayed here for the sake of brevity.
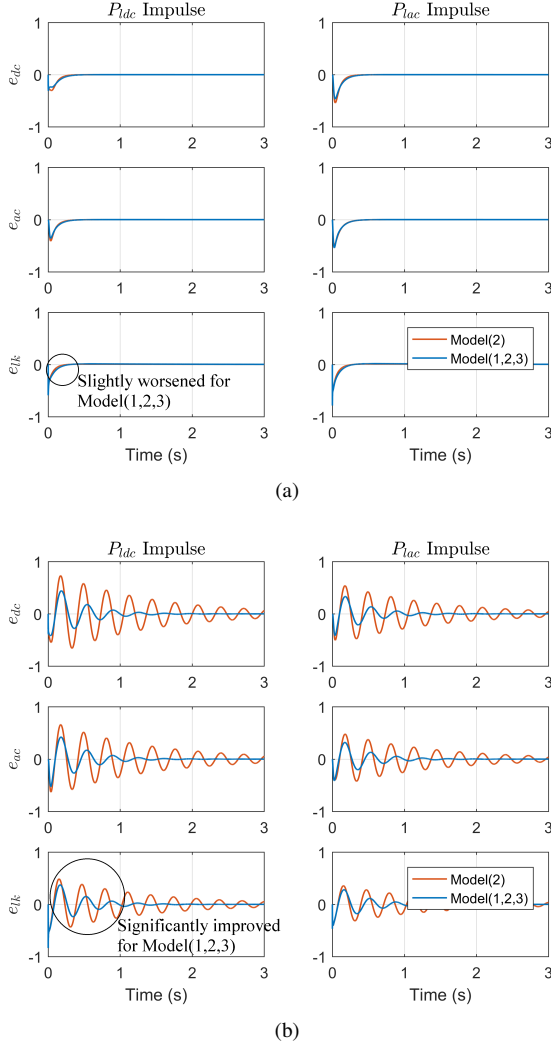

(a)

(b)

Fig. 14. Disturbance responses for optimal control gain with different model bank setting in different modes. (a) Mode2 - dc dominant. (b) Mode3 - ac dominant.

IV. SIMULATIONS AND EXPERIMENT TESTS

The performance of the transfverter and the model bank synthesis is tested in a typical ac-dc hybrid microgrid, with the system layout and parameters given in Fig. 15, Fig. 16, and Table I. Resistors R_{lac} and R_{ldc} are used to emulate ac and dc loads respectively. Z_{ac1}, Z_{dc1}, and Z_{dc2} represent the line impedance. Transformers T_{grid} and T_{inter} are used for galvanic isolation. The ac subgrid is connected to the utility grid via a switch S_{ac}, and a DG is fed into the dc subgrid via another switch S_{dc}. When both S_{ac} and S_{dc} are on, the hybrid system operates in Mode1 (balanced); when S_{ac} is off and S_{dc} is on, the system works in Mode2 (dc dominant); and when S_{ac} is on and S_{dc} is off, the system is in Mode3 (ac dominant). A relatively large interlink capacitor ($C_{lk} = 15$mF) is used in the experiment system to allow for unbalanced loads on the ac

sides without causing excessive interlink voltage ripple. The functionality of the transfverter itself is not dependent upon a bulk interlink capacitor since the voltage stiffness is transferred from the other side rather than created by the transfverter alone.
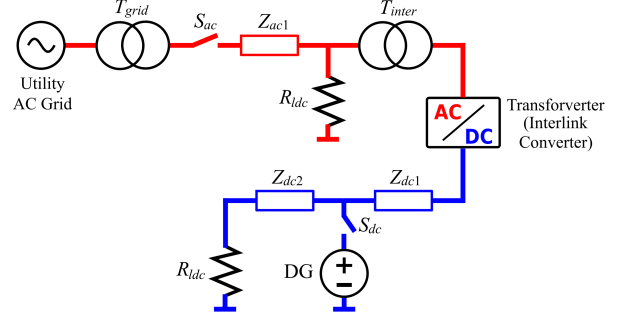

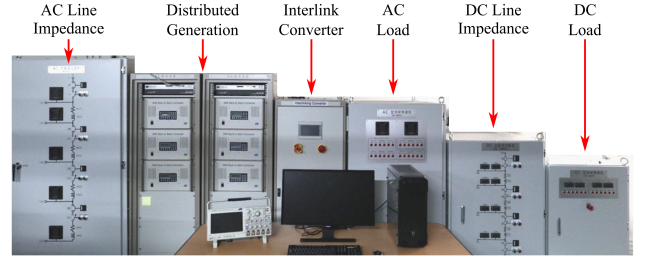Fig. 15. Layout of the tested ac-dc hybrid microgrid system.

Fig. 16. Photo of the ac-dc hybrid microgrid experiment platform.

TABLE I
KEY PARAMETERS OF TESTED AC-DC HYBRID MICROGRID SYSTEM

Network Layout	
AC Rated Voltage	$V_{ac} = 380$V (Line-Line RMS)
AC Rated Frequency	$f_{ac} = 60$Hz
Transformers	$T_{grid} = T_{inter} = 1 : 1$
AC Line Impedance	$R_{ac1} = 1.42\Omega$, $L_{ac1} = 0.6$mH
DC Rated Voltage	$V_{dc} = 380$V
DC Line Impedance	$R_{dc1} = R_{dc2} = 0.536\Omega$ $L_{dc1} = L_{dc2} = 0.026$mH
Passive Load	$R_{lac} = R_{ldc} = 240\Omega$
Interlink Converter Configuration	
Rated Power	$P_{inter} = 3$kW
AC droop gain	$D_{ac} = f_{ac}/P_{inter}/300 = 0.0667$Hz/kW
DC droop gain	$D_{dc} = V_{dc}/P_{inter}/100 = 1.27$V/kW
AC-side filter	$C_{fac} = 15\mu$F, $L_{fac} = 2$mH
DC-side filter	$C_{fdc} = 20\mu$F, $L_{fdc} = 1$mH
Interlink Capacitor	$C_{lk} = 15$mF

Two scenarios are considered in the test: DG outage on the dc side, and utility grid outage on the ac side. These scenarios not only represent typical disturbances in a practical hybrid microgrid, but also trigger the mode transition through which we can observe the dynamics of the transfverter. S_{dc} and S_{ac} are switched to generate these outages.
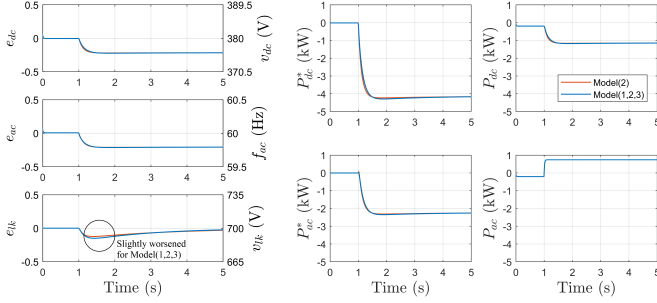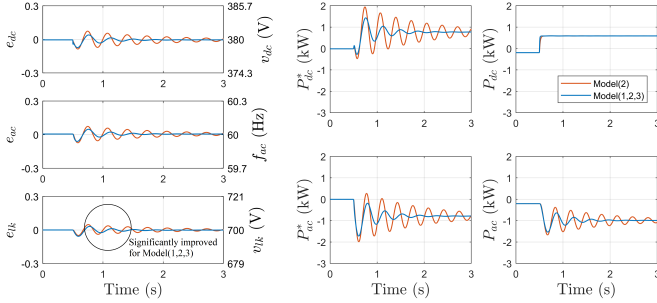
Fig. 17. Simulation results for the proposed controller gain choice (in blue) and a single-mode controller (in red). (a) AC-side utility grid outage: transition from Mode1 (balanced) to Mode2 (dc dominant) after opening switch S_{ac} at $t = 1$. (b) DC-side DG outage: transition from Mode1 (balanced) to Mode3 (ac dominant) after opening switch S_{dc} at $t = 0.5$.

Fig. 19. Experiment results using the same physical configuration and control parameters as simulation. (a) AC-side utility grid outage: transition from Mode1 (balanced) to Mode2 (dc dominant) after opening switch S_{ac} at $t = 1$. (b) DC-side DG outage: transition from Mode1 (balanced) to Mode3 (ac dominant) after opening switch S_{dc} at $t = 0.5$.
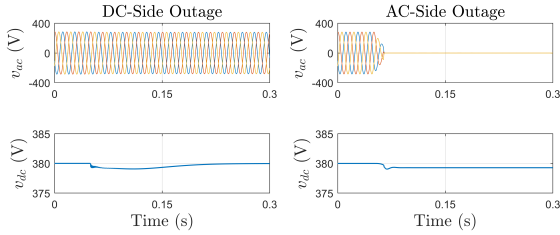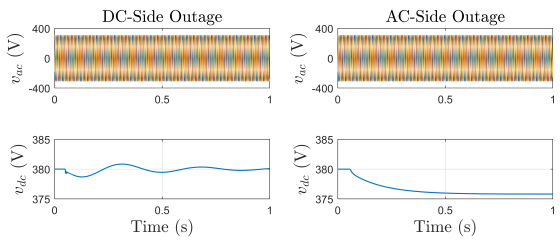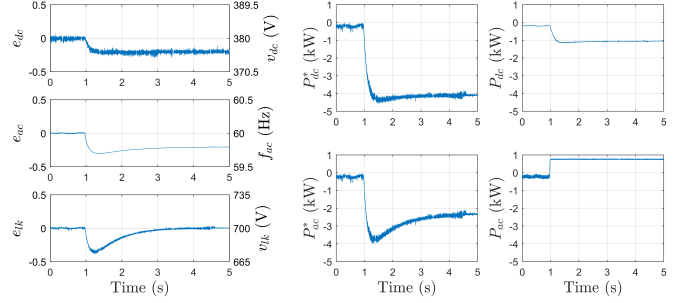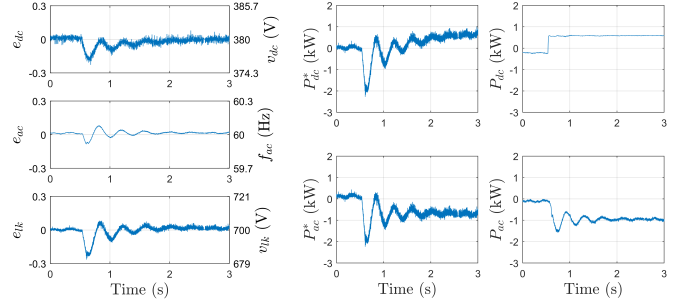

Fig. 18. Simulation results to compare transfverter with a prior-art solution. (a) Prior art: dc voltage settles fast after a dc outage but ac voltage collapses after an ac outage. (b) Transfverter: rides through both dc and ac outages with no apparent voltage disturbances, but takes a longer time to settle to equilibrium.

We first show the simulation results in Simulink in Fig. 17. For both scenarios, the dc voltage (represented by e_{dc}) and ac frequency (represented by e_{ac}) go through an initial transient variation but then settle to a new equilibrium, indicating that the transfverter stabilizes the network in mode transition. Two set of control parameters are compared. Parameters obtained

for the model bank contains all modes (Model(1,2,3)) represent the proposed solution whereas those from a model bank containing only Mode2 (Model(2)) represents a controller designed for one mode only. The response of the proposed solution to an ac outage is slightly worse than the solution designed specifically for Mode2 but the response for dc outage is significantly improved. This matches the theoretical analysis in Fig. 14 in Section III and further verifies that the model bank synthesis achieves the best overall performances across different modes.

It is interesting to note that there are significant actuation errors between the droop power set points (P_{dc}^*, P_{ac}^*) and actual power (P_{dc}, P_{ac}). This is because droop control is not error-free: the lower the droop gain (D_{dc}, D_{ac}), the higher the power error. On the other hand, lower droop gain is favored for the stiffness of voltage control. This dilemma is solved by the upper interlink controller which pushes forward the set points to compensate for the actuation error.

Further, a comparison between the proposed transfverter and a prior-art interlink scheme is presented in Fig. 18 [8], [10]. In the prior-art scheme, the ac-side converter is current controlled and the current reference is regulated to stabilize the interlink capacitor voltage, and the dc-side is voltage controlled with a droop characteristic. The direct current control enables straightforward power flow regulation between the dc and ac subgrids. It is seen to facilitate faster settlement and balancing after a dc outage, but suffer from voltage collapse after an ac outage due to the lack of direct voltage control on the ac side. In contrast, the transfverter can ride through both

dc and ac outages with no apparent voltage disturbances, at the expense of taking a longer time to settle and balance since the power flow between dc and ac subgrids is regulated indirectly by changing the droop references. Considering that voltage stability is more critical and stringent than power flow balancing, the transfverter shows a clear advantage in robustness of voltage control and immunity to mode changes (dc or ac outage). Another simulation test also validates that the transfverter still functions well if the interlink capacitor is reduced to 1.1mF, confirming that the improved performance of transfverter is caused by control rather than extra hardware. The detailed waveforms are similar to Fig. 17 and are not included in the paper for the sake of brevity. Readers interested may refer to the simulation files used to generate these results from https://spiral.imperial.ac.uk.

Experiments are conducted on a lab demonstration system with the same physical configuration and control parameters (Model(1,2,3)). The experiment results, displayed in Fig. 19, generally match the simulation, although minor differences are still observable due to imperfect modeling in the simulation. The experiments, combined with the simulation, validates the accuracy of the analysis, and the applicability of the transfverter concept in practical systems.

V. Conclusions

The concept of transfverter provides unified solution for interlink control of a hybrid ac-dc microgrid in different modes. Like a transformer, a transfverter can auto-sense the location of voltage sources and transfer the voltage stabilization capability to where it is needed, thus enhancing the voltage stability across the microgrid with a high robustness against mode transition. The model bank synthesis method identifies a single controller gain matrix that represents the best tradeoff among possibly conflicting targets and achieves the best overall performances across mode changes in the microgrid plant without requiring mode changes in the controller. Simulation and experiments results match the analysis and verify the practical applicability and effectiveness of the proposed solution.

References

[1] J. M. Guerrero, M. Chandorkar, T. Lee, and P. C. Loh, "Advanced control architectures for intelligent microgrids–part i: Decentralized and hierarchical control," *IEEE Trans. Ind. Electron.*, vol. 60, no. 4, pp. 1254–1262, Apr. 2013.

[2] J. M. Guerrero, L. C. Poh, L. Tzung-Lin, and M. Chandorkar, "Advanced control architectures for intelligentmicrogridspart ii: Power quality, energy storage, and ac/dc microgrids," *IEEE Trans. Ind. Electron.*, vol. 60, no. 4, pp. 1263–1270, Apr. 2013.

[3] T. Dragicevic, X. Lu, J. C. Vasquez, and J. M. Guerrero, "Dc microgrids–Part II: A review of power architectures, applications and standardization issues," *IEEE Trans. Power Electron.*, vol. 31, no. 5, pp. 3528–3549, May 2016.

[4] F. Nejabatkhah and Y. W. Li, "Overview of power management strategies of hybrid AC/DC microgrid," *IEEE Trans. Power Electron.*, vol. 30, no. 12, pp. 7072–7089, Dec. 2015.

[5] Y. Gu, X. Xiang, W. Li, and X. He, "Mode-adaptive decentralized control for renewable dc microgrid with enhanced reliability and flexibility," *IEEE Trans. Power Electron*, vol. 29, no. 9, pp. 5072–5080, 2014.

[6] Y. Gu, W. Li, and X. He, "Frequency-coordinating virtual impedance for autonomous power management of dc microgrid," *IEEE Transactions on Power Electronics*, vol. 30, no. 4, pp. 2328–2337, 2015.

[7] H. Lotfi and A. Khodaei, "Ac versus dc microgrid planning," *IEEE Transactions on Smart Grid*, vol. 8, no. 1, pp. 296–304, Jan 2017.

[8] P. C. Loh, D. Li, Y. K. Chai, and F. Blaabjerg, "Autonomous operation of hybrid microgrid with AC and DC subgrids," *IEEE Trans. Power Electro.*, vol. 28, no. 5, pp. 2214–2223, May. 2013.

[9] P. C. Loh, D. Li, Y. K. Chai, and F. Blaabjerg, "Autonomous control of interlinking converter with energy storage in hybrid AC–DC microgrid," *IEEE Trans. Ind. Appl.*, vol. 49, no. 3, pp. 1374–1382, May/Jun. 2013.

[10] Y. Xia, Y. Peng, P. Yang, M. Yu, and W. Wei, "Distributed coordination control for multiple bidirectional power converters in a hybrid AC/DC microgrid," *IEEE Trans. Power Electro.*, vol. 32, no. 6, pp. 4949–4959, Jun. 2017.

[11] H. Xiao, A. Luo, Z. Shuai, G. Jin, and Y. Huang, "An improved control method for multiple bidirectional power converters in hybrid AC/DC microgrid," *IEEE Trans. Smart Grid*, vol. 7, no. 1, p. 340347, Jan. 2016.

[12] H. Zhang, J. Zhou, Q. Sun, J. M. Guerrero, and D. Ma, "Data-driven control for interlinked ac/dc microgrids via model-free adaptive control and dual-droop control," *IEEE Transactions on Smart Grid*, vol. 8, no. 2, pp. 557–571, 2017.

[13] X. Feng, J. Liu, and F. C. Lee, "Impedance specifications for stable DC distributed power systems," *IEEE Trans. Power Electron.*, vol. 17, no. 2, pp. 157–162, Mar. 2002.

[14] J. Sun, "Impedance-based stability criterion for grid-connected inverters," *IEEE Trans. Power Electron.*, vol. 26, no. 11, pp. 3075–3078, Nov. 2011.

[15] X. Liu, P. Wang, and P. C. Loh, "A hybrid AC/DC microgrid and its coordination control," *IEEE Trans. Smart Grid*, vol. 2, no. 2, pp. 278–286, Jun. 2011.

[16] L. Che, M. Shahidehpour, A. Alabdulwahab, and Y. Al-Turki, "Hierarchical coordination of a community microgrid with AC and DC microgrids," *IEEE Trans. Smart Grid*, vol. 6, no. 6, pp. 3042–3051, Nov. 2015.

[17] J. Rocabert, A. Luna, F. Blaabjerg, and P. Rodriguez, "Control of power converters in AC microgrids," *IEEE Trans. Power Electron.*, vol. 27, no. 11, pp. 4734–4749, Nov. 2012.

[18] F. Gao, S. Bozhko, A. Costabeber, C. Patel, P. Wheeler, C. I. Hill, and G. Asher, "Comparative stability analysis of droop control approaches in voltage-source-converter-based DC microgrids," *IEEE Trans. Power Electron.*, vol. 32, no. 3, pp. 2395–2415, Mar. 2017.

[19] J. Kim, J. M. Guerrero, R. T. P. Rodriguez, and K. Nam, "Mode adaptive droop control with virtual output impedances for an inverter based flexible ac microgrid," *IEEE Trans. Ind. Electron.*, vol. 26, no. 3, pp. 689–702, Mar. 2011.

[20] X. Wang, Y. W. Li, F. Blaabjerg, and P. C. Loh, "Virtual-impedance based control for voltage-source and current-source converters," *IEEE Trans. Power Electron.*, vol. 30, no. 12, pp. 7019–7037, Dec. 2015.

[21] J. V. de Vyver, J. D. M. D. Kooning, B. Meersman, L. Vandevelde, and T. L. Vandoorn, "Droop control as an alternative inertial response strategy for the synthetic inertia on wind turbines," *IEEE Transactions on Power Systems*, vol. 31, no. 2, pp. 1129–1138, March 2016.

[22] S. D'Arco and J. A. Suul, "Equivalence of virtual synchronous machines and frequency-droops for converter-based microgrids," *IEEE Transactions on Smart Grid*, vol. 5, no. 1, pp. 394–395, Jan 2014.

[23] Y. W. Li and C.-N. Kao, "An accurate power control strategy for power-electronics-interfaced distributed generation units operating in a low-voltage multibus microgrid," *IEEE Transactions on Power Electronics*, vol. 24, no. 12, pp. 2977–2988, 2009.

[24] Y. Gu, N. Bottrell, and T. C. Green, "Reduced-order models for representing converters in power system studies," *IEEE Transactions on Power Electronics*, vol. 33, no. 4, pp. 3644–3654, 2018.

[25] Y. Gu, Y. Li, and T. C. Green, "Impedance/admittance modeling of three-phase ac systems: A general representation," *arXiv preprint arXiv:1810.09911*, 2018.

[26] J. Rocabert, A. Luna, F. Blaabjerg, and P. Rodriguez, "Control of power converters in ac microgrids," *IEEE transactions on power electronics*, vol. 27, no. 11, pp. 4734–4749, 2012.

[27] M. Green and D. J. Limebeer, *Linear robust control*. Courier Corporation, 2012.

[28] M. J. Osborne and A. Rubinstein, *A course in game theory*. MIT press, 1994.

[29] D. P. Bertsekas and A. Scientific, *Convex optimization algorithms*. Athena Scientific Belmont, 2015.

Yunjie Gu (M'18) received the B.Sc. and the Ph.D. degree in Electrical Engineering from Zhejiang University, China, in 2010 and 2015 respectively. He was a Consultant at General Electric Global Research Centre (Shanghai) from 2015 to 2016, and is now a Research Fellow at Imperial College London, UK, sponsored by UK Research and Innovation (UKRI) Fellowships. His research interests include modeling, analysis and control of power-electronic-enabled low-carbon power networks.
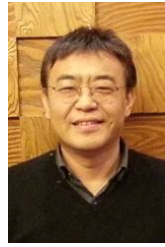
Hak-Man Kim (SM'15) received his first Ph.D. degree in Electrical Engineering from Sungkyunkwan University, Korea in 1998 and received his second Ph.D. degree in Information Sciences from Tohoku University, Japan, in 2011, respectively. He worked for Korea Electrotechnology Research Institute (KERI), Korea from Oct. 1996 to Feb. 2008. Currently, he is a professor in the Department of Electrical Engineering, Incheon National University, Korea. His research interests include microgrid operation, control and DC power systems.

Yitong Li (S'17) received the B.Eng degrees from Huazhong University of Science and Technology, China, and the University of Birmingham, UK, in 2015. He received his M.Sc degree in Future Power Networks from Imperial College London, UK, in 2016, where he is currently pursuing his Ph.D. degree. His current research interests include control techniques and power electronic converters for power distribution applications.

Adria Junyent-Ferre (S'09-M'19) obtained his Industrial Engineering degree from the School of Industrial Engineers of Barcelona (ETSEIB), Polytechnic University of Catalonia (UPC) in 2007, and the Ph.D. in Electrical Eng. from the UPC in 2011. He was a Researcher at CITCEA-UPC from 2006 to 2012 and a Lecturer at the Barcelona College of Industrial Engineering (EUETIB) in 2012. He joined the Dept. of Electrical and Electronic Eng. at Imperial College London in 2013 and became a Lecturer in 2014. His research focuses on control of power electronic converters and their design, with specific focus on wind power, VSC-HVDC and microgrids.

Hyeong-Jun Yoo (M'18) received his Ph.D. degree in Electrical Engineering from Incheon National University (INU), Korea, where he is presently working as a Postdoctoral Researcher. His current research interests include the control of power conversion systems, microgrids and dc distribution systems.

Thai-Thanh Nguyen (M'19) received his B.S degree in Electrical Engineering from Hanoi University of Science and Technology, Vietnam, in 2013. Currently, he is a Ph. D. student in the Department of Electrical Engineering, Incheon National University (INU), Korea. His research interests include power converter control, microgrid, and power system analysis.

Timothy C. Green (M'89-SM'02-F'19) received a B.Sc. (Eng) (first class honors) from Imperial College London, UK in 1986 and a Ph.D. from Heriot-Watt University, UK in 1990. He is a Professor of Electrical Power Engineering at Imperial College London, and Director of the Energy Futures Lab with a role of fostering interdisciplinary energy research across the university. His research uses the flexibility of power electronics to create electricity networks that can accommodate greater amounts of low carbon technologies. In HVDC, he has contributed converter designs that strike improved trade-offs between power losses, physical size and fault handling. In distribution systems, he has pioneered the use of soft open points and the study of stability of grid connected inverters. He is a Chartered Engineering in the UK and a Fellow of the Royal Academy of Engineering.

Xin Xiang (M'18) received the B.Sc. degree in Electrical Engineering from Harbin Institute of Technology, China in 2011 and the M.Sc. degree in Electrical Engineering from Zhejiang University, China in 2014. In 2018, he received the Ph.D. degree from the Department of Electronical and Electronic Engineering in Imperial College London, UK, where he is currently working as a Research Associate. His research interests include the design and control of power conversion systems for high-voltage and medium-voltage grid applications.